Enhanced desalination performance of poly (vinyl alcohol)/carbon nanotube composite pervaporation membranes via interfacial engineering

Yang, Guang, Xie, Zongli, Cran, Marlene, Ng, D and Gray, Stephen (2019) Enhanced desalination performance of poly (vinyl alcohol)/carbon nanotube composite pervaporation membranes via interfacial engineering. Journal of Membrane Science, 579. pp. 40-51. ISSN 0376-7388

Enhanced desalination performance of poly (vinyl alcohol) / carbon nanotube composite pervaporation membranes via interfacial engineering

Guang Yang [a,b], Zongli Xie [b,*], Marlene Cran [a], Derrick Ng [b], Stephen Gray [a,*]

[a] *Institute for Sustainable Industries and Liveable Cities, Victoria University, PO Box 14428, Melbourne, Vic. 8001, Australia.*

[b] *CSIRO Manufacturing, Private Bag 10, Clayton South, Vic. 3169, Australia.*

Corresponding authors:

** Email：stephen.gray@vu.edu.au; Tel. +61-3-9919-8097*

** Email: zongli.xie@csiro.au; Tel. +61-3-9545-2938.*

Abstract

The dispersion and interfacial interactions between nanofillers and the polymer are two crucial factors affecting the performance of mixed matrix membranes (MMMs). In this study, poly (vinyl alcohol) (PVA) based mixed matrix membranes containing multiwalled carbon nanotubes (MWCNTs) or carboxylic multiwalled carbon nanotubes (C-MWCNTs) were produced via interfacial adhesion, hydrogen bonding or covalent bonding. The desalination performances of the synthesised membranes were compared by the pervaporation (PV) process. A PVA membrane crosslinked with maleic acid (MA) was also prepared for comparison. SEM and TEM images indicated that the C-MWCNTs were disentangled and dispersed uniformly in the PVA matrix whereas MWCNTs without functional groups readily aggregated. The incorporation of CNTs endowed the PVA/CNT membranes with improved thermal stability, which was confirmed using TGA and DSC measurements. In particular, the altered properties of the PVA/CNT composites enhanced the separation performance compared with the PVA membrane without CNTs. The performance tests showed that the PVA/CNT composite membranes

featured remarkably larger water fluxes than control PVA/MA membrane (38.8% to 154.1% increase) while maintaining high salt rejection. Thereinto, the overall best performance of 99.91% of salt rejection and 6.96 kg/m^{2}h of water flux at room temperature (22 °C) was ~~realized~~ obtained by the PVA/C-MWCNT/MA membrane (19 ± 1 μm thickness) when the feed was synthetic NaCl solution of 35,000 ppm. Kinetic desorption method was applied to compare salt transport properties of the resultant PVA/CNT composite membranes. The salt transport through the PVA/C-MWCNT and PVA/C-MWCNT/MA membranes was significantly restricted with CNT mass fraction. High retention of water flux and salt rejection rates were also obtained by the PVA/C-MWCNT/MA membrane over a 30-hour durability test that processed seawater collected from Brighton Beach (Melbourne, VIC, Australia), while the salt rejection for the PVA/C-MWCNT membrane declined with extended operating time indicating that cross-linking of the PVA was necessary for stable MMM performance.

Keywords: Pervaporation; carbon nanotube; poly vinyl alcohol; desalination; interfacial interaction.

1. Introduction

Desalination using membrane technology which allows an effective separation of water molecules and ions by processes such as pressure driven [1, 2], electrically driven [3], thermally driven [4-6], etc., has been attractive to researchers for combating water scarcity since 1970s [1]. Pervaporation (PV), as one of the current membrane technologies, utilizes vapor pressure difference as the driving force. It is considered to be promising for water desalination [7] because it may use waste heat to drive the process, has high salt rejection irrespective of concentration and is fouling resistant [8].

Transport through PV membranes is usually explained by the solution-diffusion model, which involves dissolving of a solute or solvent in a dense membrane, permeation through the membrane and evaporation on the permeate side [9, 10]. The solute or solvent exhibits a phase change across the pervaporation membrane and is quite different to nanofiltration (NF) [2] and reverse osmosis processes (RO) [11] where pressure provides the driving force for water transportation. The PV process is similar to vacuum membrane distillation (MD) except that the membrane also plays a role in the separation of feed components, whereas for MD the separation is based solely on the vapour-liquid equilibrium relationship [4].

As the membrane has an active role in the separation process, the performance is strongly related to membrane characteristics including the morphology and chemistry. Over the past several years, increased effort has been made to fabricate novel PV desalination membranes such as inorganic membranes [12], polymeric membranes [13] and mixed matrix membranes (MMMs) [14]. In particular, MMMs, which refer to composite membranes containing a dispersed phase of inorganic entities embedded in a continuous host polymer matrix, are dominated owing to their easy fabrication, a great variety of potential fillers and the altered physicochemical properties [15]. The synergy between the polymer and filler mixtures often provides a combined separation property with enhanced perm-selectivity [16, 17], which has aroused great interest in the PV desalination process. Proper selection of the dispersed inorganic phase and the continuous matrix phase based on their intrinsic transport properties~~, thereby,~~ is therefore important. When considering which polymer would be suitable for use as the matrix, the required characteristics are: good chemical stability, easy to process, high hydrophilicity and fouling resistance [18] [19]. Poly (vinyl alcohol) (PVA) has these characteristics but is water soluble. Therefore, it should be modified to avoid dissolution in water during the PV

process [20].

Recently, a range of fillers, such as zeolites[21], silica [14], TiO_2 [22], carbon molecular sieves [23], metal-organic framework (MOF) [24], graphene oxide [25, 26] and carbon nanotubes (CNTs) [27] have been added to polymer matrices, which enable MMMs to exhibit high separation performance with improved mechanical and thermal properties. Among those various fillers, CNTs attract a great deal of attention from researchers [28]. As a one-dimensional nanomaterial, CNTs are hollow cylindrical structures with internal diameters in the nanometre range with high aspect ratio [29]. More importantly, due to their hydrophobic nature and smooth surface, CNTs lower mass transfer resistance, thus enabling fast fluid transport [30-32]. The incorporation of CNTs or functionalized CNTs into PES ultrafiltration (UF) membrane, polyamide RO membrane and polyvinylidene fluoride (PVDF) MD membrane has made obvious improvements in the permeation flux [33-35]. For example, Chan et al. [36] showed that zwitterionic functionalized CNTs in polyamide matrix produced a high water flux while rejecting essentially all ions. Furthermore, CNTs, alone, also exhibit desalination ability when they are functionalised. Corry [37] studied desalination using different functional groups at the mouth of CNTs, such as $-COO^-$, $-NH_3^+$ and -OH, and concluded that steric hinderance and electrostatic repulsion are the main reasons for preventing the passage of ions. Up to date, to the best of knowledge of the authors, there are no reports of MMMs containing CNTs that have been applied in desalination by PV. Most importantly, the interfacial interactions between the PVA and CNTs eventually determine the chemistry and performance of membrane, which requires further investigation [38].

Herein, the characteristics and performance of PVA/CNT MMMs with different interfacial interactions for PV desalination are reported. Three types of PVA/CNT membranes were developed

and compared, i.e. PVA/multiwalled carbon nanotube (MWCNT), PVA/ carboxylic MWCNT (C-MWCNT) and crosslinked PVA/C-MWCNT/maleic acid (MA) membranes. A PVA membrane crosslinked with only MA was also prepared for comparison. In general, CNTs are oxidatively modified by attaching functional groups such as -COOH and -OH on the sidewalls to enhance hydrophilicity and compatibility with the polymer. However, turning the CNTs from hydrophobic to hydrophilic means shortening the aspect ratio and the predominant part of the pristine graphitic structure is damaged by defects, resulting in a rough and disordered carbon structure [33]. That phenomenon may impede and trap water molecules. Therefore, there is a trade-off between the functionalization and applicability of CNTs with polymer. The functionalized CNTs in this research were commercial C-MWCNTs, which were not highly oxidized and were amphiphilic with a significant proportion of graphitic structure remaining. The changes to the polymer phase following incorporation of nanofillers were investigated and detailed characterisation of the membranes was undertaken to identify a potential structure-property relationship. Salt transport properties through PVA/CNT membranes were also compared using the kinetic desorption method.

2. Experimental

2.1. Materials

PVA (98-99% hydrolysed, average molecular weight of 160,000), MA, ethanol, p-toluene sulfonic acid (98.5%, monohydrate) and sodium chloride (NaCl) were purchased from Sigma-Aldrich and used without further purification. The MWCNTs and C-MWCNTs (3.86 wt% of carboxyl groups with respect to MWCNT) with diameter ranging from 2-5 nm, and specific surface area > 500 m^2/g

were obtained from XFNANO CO. Ltd. Seawater was collected from Brighton Beach, Melbourne, VIC, Australia. The electrical conductivity was 51.2 mS/cm and the pH was 8. The main cations contained in the seawater were Ca^{2+}, Mg^{2+}, Na^{+} and K^{+} and the corresponding mass concentrations were 412 ppm, 1,272 ppm, 10,787 ppm and 397 ppm. Milli-Q deionised water (18.1 MΩ cm at 25 °C) was used to prepare the PVA and aqueous NaCl solutions.

2.2. Preparation of PVA/CNT membranes

The PVA powder (6 g) was added to 100 mL of Milli-Q deionised water at 90°C with stirring until fully dissolved. The obtained 6 wt% PVA viscous solution was then left to cool to room temperature (22°C). A mass of 200 mg of MWCNTs or C-MWCNTs were added to 100 mL of ethanol and then sonicated in an ice bath for 2 h. Blending of the PVA/MWCNT or PVA/C-MWCNT was achieved by dropwise addition of a specified amount of MWCNT or C-MWCNT dispersion to the PVA solution. For the PVA/C-MWCNT/MA membrane, 20 wt% of MA and 1.5 wt% of p-toluene sulfonic acid as catalyst were added to the mixture under stirring [14] [39]. All the mass fractions of CNTs, MA and p-toluene sulphonic acid are with respect to the mass of PVA. After vigorous stirring for 2 h, the PVA/CNT mixtures were subjected to ultrasonication for 30 min. The resultant homogeneous mixtures of the PVA/MWCNT, the PVA/C-MWCNT and the PVA/C-MWCNT/MA were then degassed and cast on Perspex petri dishes followed by air drying. Once dried, the obtained membranes were peeled off and annealed at 140 °C for 2 h. The thicknesses of all the membranes were 19 ± 1 um measured by a Fowler electronic digital micrometre. For comparison, a PVA/MA membrane with the same thickness was also prepared as a control. The synthesis of PVA/CNT membrane is schematically illustrated in Fig.1.

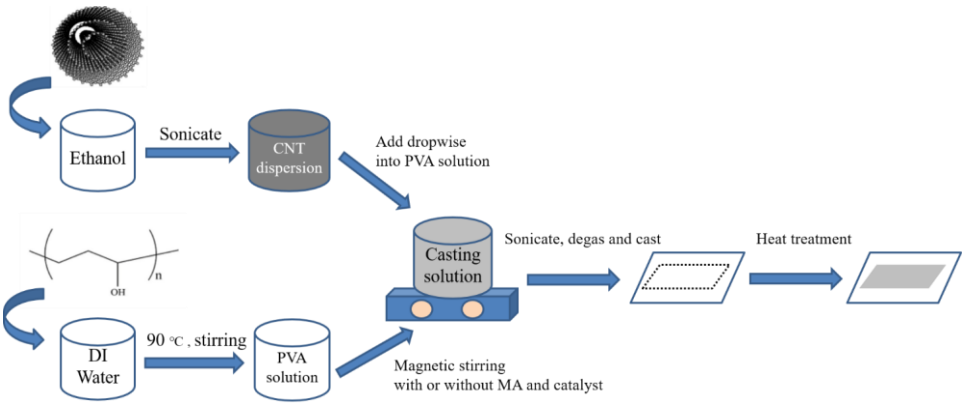

Fig. 1. Synthesis process of PVA/CNT composite membranes.

2.3. Membrane characterisation

The functional structure of fabricated membrane samples was assessed by attenuated total reflectance-Fourier transform infrared (ATR-FTIR) spectroscopy using a Perkin-Elmer Spectrum 2000 FTIR instrument (USA). The crystalline size of the membranes was studied using a Bruker D8 advanced wide-angle X-ray diffractometer (WAXD) with Cu-K radiation (40 kV, 40 mA). Both the surface and cross-section morphologies of the membrane samples were imaged by Zeiss Merlin Gemini 2 Field Emission Scanning Electron Microscopy (FESEM). The TECNAI 12 transmission electron microscope (TEM) under an accelerating voltage of 200 kV was used to observe the CNTs dispersion in the polymer matrix. Thermogravimetric analysis (TGA) and differential scanning calorimetry (DSC) were performed on a PerkinElmer Pyris instruments under nitrogen at a heating rate of 10 °C per minute. The temperature range for TGA was from 30 to 800 °C. The DSC analysis was conducted with samples of approximately 5-10 mg over the temperature range of 10 to 250 °C. Melting enthalpy (ΔH) values were calculated by numerical integration of the area under the melting peaks (ΔH_m) and the degree of crystallinity (X_c) was calculated from the ratio between melting

enthalpy of the samples and melting enthalpy of PVA with 100% crystallinity, ΔH_0, as shown in Eq (1). A value of 138.6 J/g was assumed for ΔH_0 in accordance with [40].

$$X_c = \frac{\Delta H_m}{\Delta H_0} \quad (1)$$

Contact angle measurements were performed using a KSV contact angle meter (CAM200) equipped with an image capturing system. For the swelling properties, dried films were immersed in DI water at room temperature for 48 h to reach absorption equilibrium. After gentle dab drying of the water drops off the surface with tissues, the mass of the film, W_s, was measured and recorded as the wet weight before the sample was dried in a vacuum oven at 50 °C overnight and weighed again to obtain the dry weight, W_d. The degree of swelling (S) was then calculated using Eq (2);

$$s = \frac{w_s - w_d}{w_d} \times 100\% \quad (2)$$

2.4. Pervaporation performance test

Performance tests were carried out using a laboratory scale PV unit as described in previous studies [14]. A membrane was placed in the middle of a PV cell with an effective transport area of 12.6 cm^2. Synthetic NaCl solution (3.5 wt%) or seawater was used as the feed solution which was preheated in a water bath to the required temperature and pumped to the PV cell by a Masterflex® peristaltic pump. The flow rate of the feed was maintained at 50 mL/min. A K-type thermocouple was installed in the feed chamber to monitor the operating feed temperature. Absolute pressure applied on the permeate side of the membrane cell was maintained at 6 Torr using a vacuum pump and the permeate was collected in a dry-ice cold trap. In this study, it was observed that a minimum of 30 min was required to reach membrane performance stability. The performance test using NaCl aqueous solutions

as feed was conducted for 3 h whereas the long-term stability test using seawater lasted for 30 h. The water flux (J) was determined from the mass (M) of permeate collected in the cold trap, the effective membrane area (A) and the experimental time (t). The salt concentration of the feed (C_f) and permeate (C_p) were derived from a pre-calibrated Oakton® Con 110 conductivity meter. The pervaporation desalination performance was evaluated by J and salt rejection (R), which were calculated by the following equations, respectively;

$$J = \frac{M}{A \times t} \tag{3}$$

$$R = \frac{C_f - C_p}{C_f} \times 100\% \tag{4}$$

It should be noted that at the end of each experiment, the permeate side of the membrane cell was flushed with a known amount of de-ionised water and the conductivity of this stream was taken into account for the overall salt rejection.

2.5. Salt transport properties

The NaCl transport properties of membranes were determined by the kinetic desorption method [41, 42]. The desorption results were fitted to the Fickian diffusion model to calculate the NaCl diffusivity, D_s in the membrane by plotting (M_t/M_∞) versus $t^{1/2}$ using Eq (5).

$$D_S = \frac{\pi \times l_W^2}{16}\left[\frac{d\left(\frac{M_t}{M_\infty}\right)}{d\left(t^{\frac{1}{2}}\right)}\right]^2 \tag{5}$$

where M_t is the amount of NaCl in the solution at time t and M_∞ is the total amount of NaCl desorbed from the membrane into the solution, and l_w is the thickness of the hydrated membrane.

The NaCl solubility, K_s, is the ratio of equilibrium amount of NaCl absorbed into the membrane

per unit membrane volume to the concentration of NaCl in the original solution [41]. According to the solution-diffusion model, NaCl permeability, P_s, is the product of D_s and K_s.

$$P_s = D_s \times K_s \tag{6}$$

3. Results and discussion

3.1. Dispersion of CNTs in the PVA matrix

A critical factor affecting the performance of MMMs is the dispersion of nanofillers in the polymer matrix [28]. For CNTs, there are not only Van der Waals interactions forcing them to agglomerate but also π–π interactions [43]. Fig. 2 shows the TEM images of the dispersion of MWCNTs and C-MWCNTs in cross-sectioned PVA/MWCNT and PVA/C-MWCNT membranes.

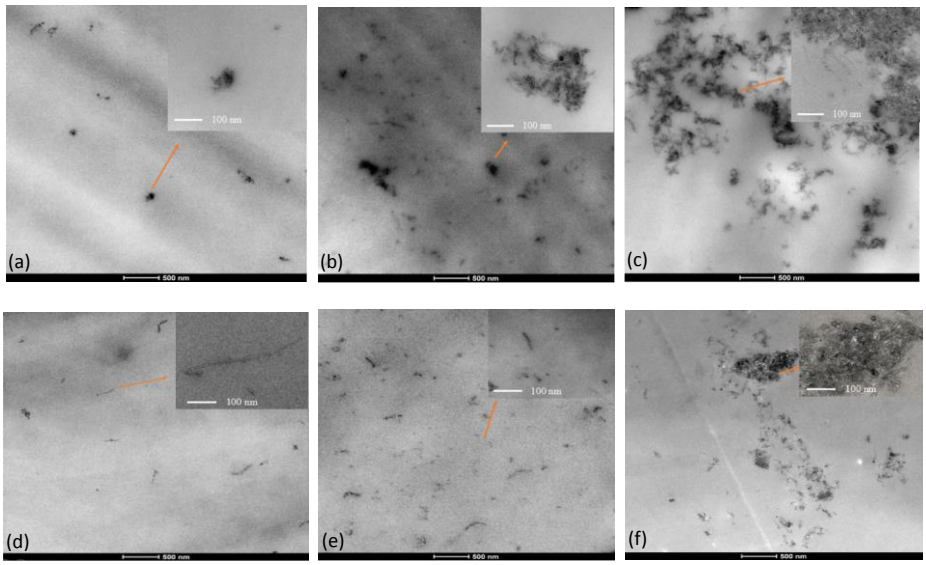

Fig. 2. Cross-sectioned PVA/MWCNT and PVA/C-MWCNT composites with different CNTs loading: (a) 0.5 wt% MWCNTs; (b) 1 wt% MWCNTs; (c) 2 wt% MWCNTs; (d) 0.5 wt% C-MWCNTs; (e) 1 wt% C-MWCNTs and (f) 2 wt% C-MWCNTs. Main scale-bar is 500 nm and inserted scale-bar is 100 nm.

As shown in Fig. 2a, 2b and 2c, the dispersion states of MWCNTs varied significantly with their concentrations in the PVA matrix and phase separation was clearly evident with addition of CNTs. Although the PVA can wet CNTs [44], MWCNTs lack strong interfacial affinity with the PVA due to the physical blending of CNTs and PVA. As a result, MWCNTs were randomly distributed in clumps from 0.5 wt% to 1 wt%. The phase separation became more severe and there were large entanglements when MWCNTs mass fraction reached 2 wt%. In contract, C-MWCNTs were more compatible with the PVA matrix. The images showed that C-MWCNTs were disentangled and uniformly distributed in the polymer matrix. Single nanotubes were immobilized in the polymer matrix as shown in Fig. 2d and 2e. However, there were still agglomerated nanotubes when the C-MWCNT loading was increased to 2 wt% in Fig. 2f due to the decreased distance between each C-MWCNT.

The corresponding surface SEM pictures of the PVA/MA, PVA/MWCNT and PVA/C-MWCNT membranes are presented in Fig. 3. The PVA/MA membrane was a dense membrane with a smooth and nonporous surface. After the addition of MWCNTs, fibre-shaped protrusions and dots similar to CNT tips [27] were observed on the surface of PVA/MWCNT membranes as shown in Fig. 3b and 3c. Increasing the MWCNT loading resulted in a greater number of pinnacles and entangled lumps on the surface, which was mainly due to the increased agglomeration of MWCNTs. These observations are also consistent with the TEM results described in Fig. 2. Compared with the PVA/MWCNT membrane, the morphology of PVA/C-MWCNT membrane was much more uniform. A few fibre shaped protrusions, which represented the CNT tips, and interspersed bundle-like shapes only appeared when 2 wt% C-MWCNTs were incorporated as shown in Fig. 3e. Fig. 3f and 3g show the cross-sectioned PVA/CNT membranes and unsurprisingly, for the PVA added with non-functionalised CNT, agglomerates and large bundles of protruding MWCNTs sit within the matrix of PVA/MWCNTs

membrane. Conversely, the C-MWCNT incorporated PVA membrane has a homogeneous and smooth interior structure.

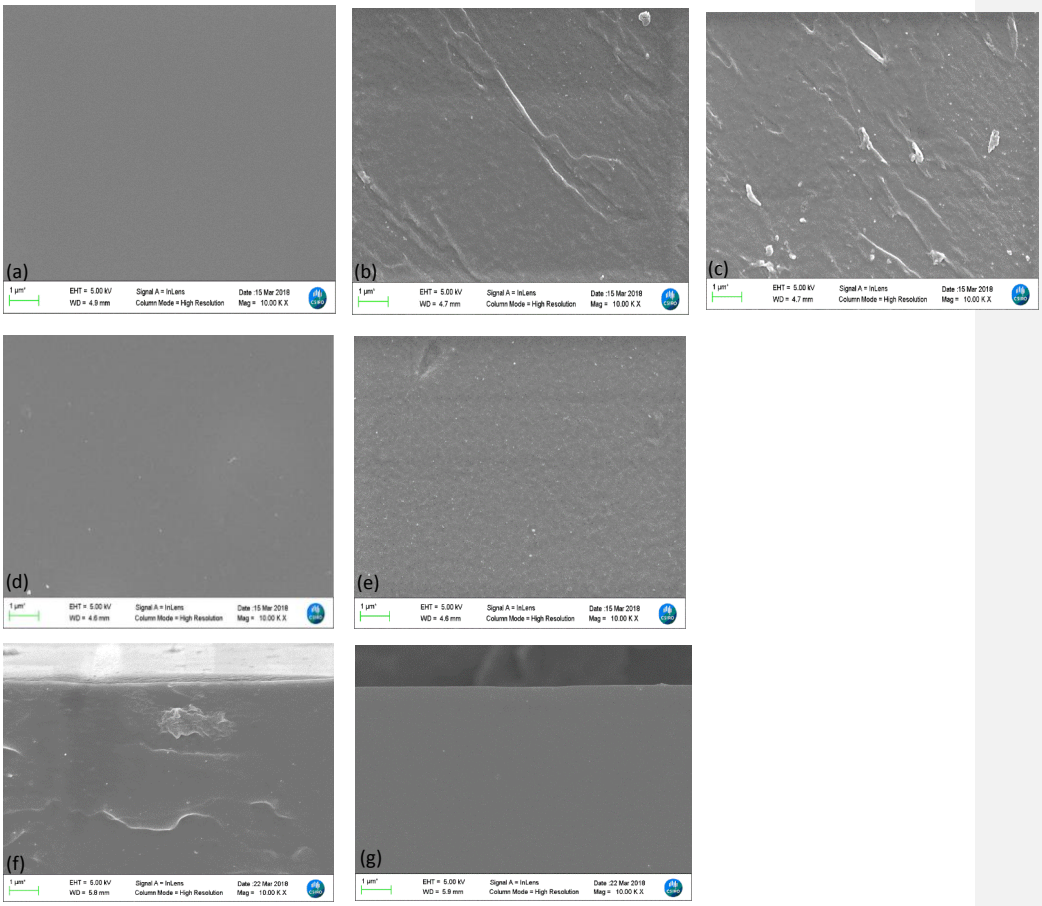

Fig. 3. SEM top surface of the synthesized membranes with different CNTs loading; (a) PVA/MA; (b)1 wt% MWCNTs; (c) 2 wt% MWCNTs; (d) 1% C-MWCNTs and (e) 2% C-MWCNTs. Cross-sectional view of the membranes with different CNTs loading; (f) 1wt% MWCNTs and (g) 1wt% C-MWCNTs. Scale-bar is 1 µm.

3.2. Interactions between CNTs and PVA

Fig. 4 shows the ATR-FTIR spectra of the different membrane samples where each PVA/CNT sample contained 1 wt% of MWCNTs or C-MWCNTs with respect to PVA. For all spectra, the peaks

appeared in 3000-3500 cm^{-1} region were the characteristic peaks of the hydrogen-bonded hydroxyl group of the PVA polymer. Alkyl peaks, which are assigned to the stretching vibrations of C-H group in the PVA backbone, were characterized at the wave numbers of 2960 cm^{-1} and 2914 cm^{-1}, and the sharp C-OH stretching peaks from PVA matrix were observable at 1085 cm^{-1}.

For the control PVA membrane, PVA/MWCNT membrane and PVA/C-MWCNT membrane, the spectra were almost identical. The MWCNTs without functional groups, theoretically, should pose no change of chemical bonding to the PVA matrix when incorporated into the polymer matrix. The MWCNTs mainly interacted with the surrounding PVA polymer matrix via interfacial adhesion, which included physical interactions and mechanical interlocking [44]. The interaction scheme of MWCNTs and PVA is presented in Fig. 5a. In opposition, the -COOH entities that were covalently attached to the carbon sidewalls could form hydrogen bonding with the -OH groups from the PVA [27]. Therefore, the compatibility between C-MWCNTs and PVA would be enhanced due to stronger interfacial interactions as illustrated in Fig. 5b.

A PVA/C-MWCNT without MA was also prepared to investigate if there was an esterification reaction between C-MWCNT and PVA. As can be seen, characteristic peaks of ester groups (i.e. C=O at 1720 cm^{-1} and two C-O bands at 1330-1050 cm^{-1} with a strong peak at higher wavenumbers and a weak peak at lower wavenumbers) appeared. This confirmed that esterification reaction had taken place, probably during the heat treatment process. The same esterification peaks were also visible for PVA/MA, which confirmed that PVA was successfully crosslinked with MA via esterification reaction [14]. PVA/C-MWCNT/MA exhibited the strongest IR absorption of the ester groups, which may imply that PVA was crosslinked with both C-MWCNT and MA. Additionally, the decrease of peak intensity in 3000-3500 cm^{-1} region due to the consumption of the hydrogen-bonded hydroxyl group also

confirmed that increased esterification occurred for the PVA/C-MWCNT/MA membrane. As a comparison, the blended membrane samples had stronger hydrogen-bonded hydroxyl peaks than crosslinked samples, suggesting that large amount of hydroxyl groups from PVA remained. The reaction schemes of crosslinked PVA membrane are shown in Fig.5c and 5d which show that PVA and C-MWCNT or MA form covalent bonds between carboxylic group and hydroxy by dehydration condensation, thus forming an interconnected network.

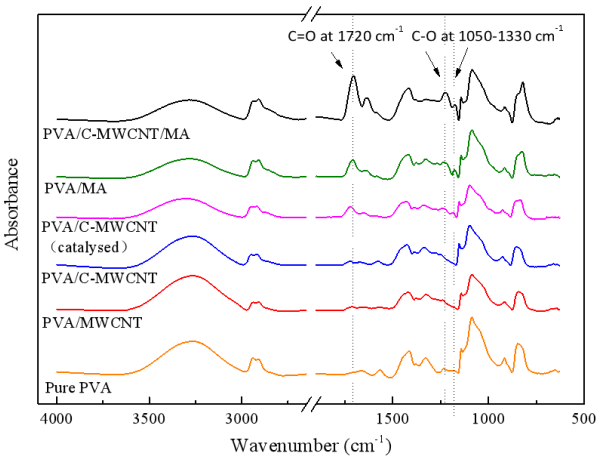

Fig. 4. FTIR spectra of the synthesized membranes.

(a)

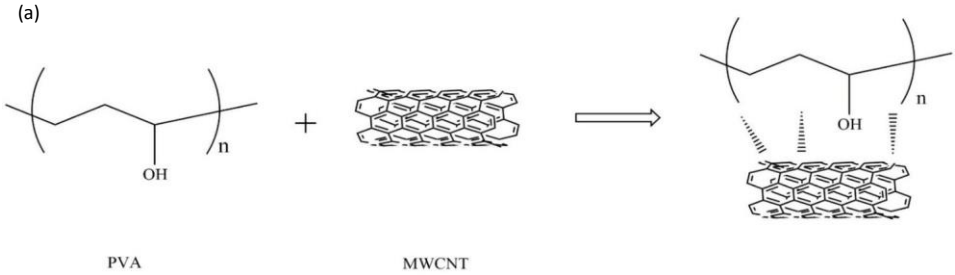

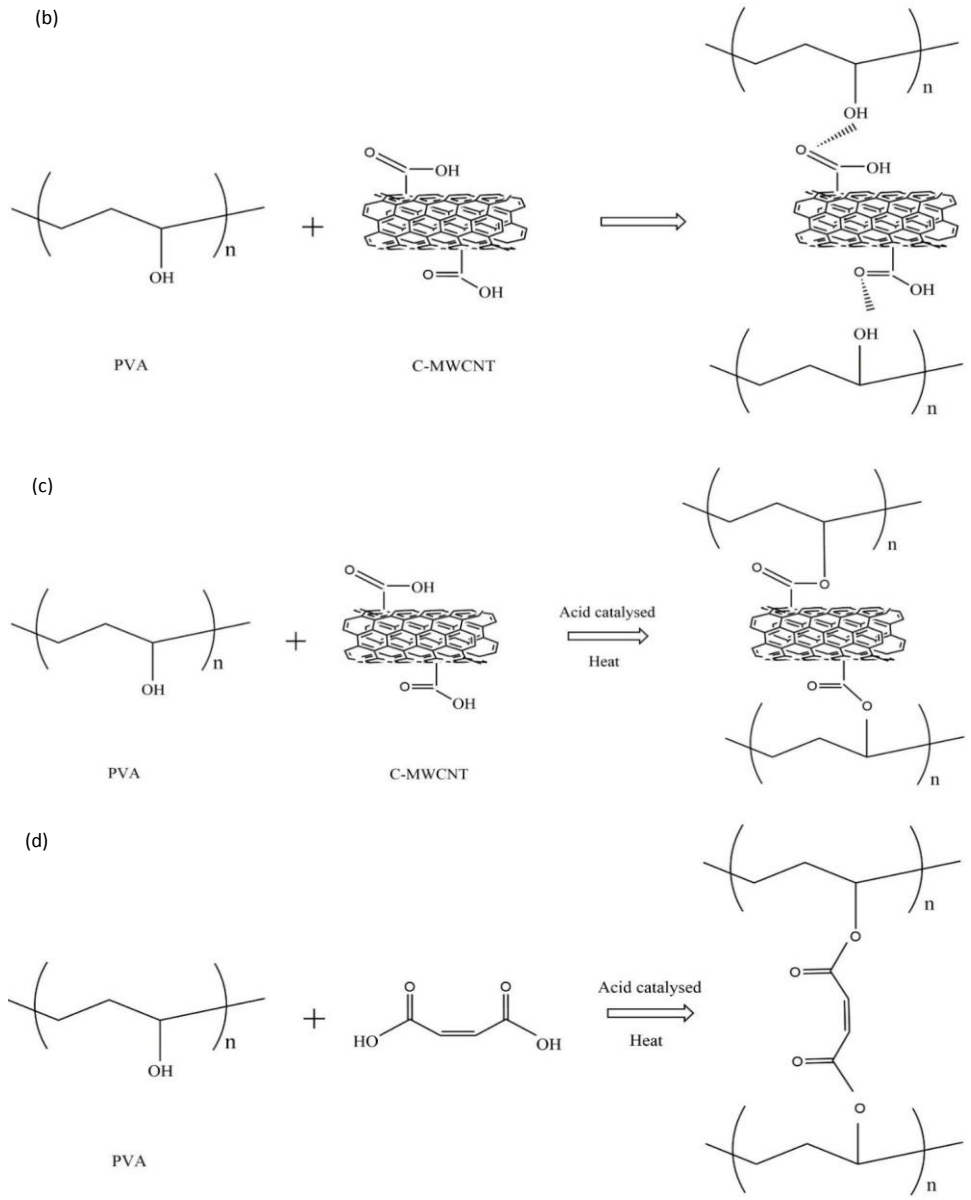

Fig. 5. Reaction and interaction scheme: (a) Van der Waals force between PVA and MWCNT; (b) Hydrogen bonding between PVA and C-MWCNT; (c) and (d) Esterification reactions between PVA and C-MWCNT and MA.

3.3. Effects of CNTs on the PVA matrix

3.3.1. Effects of CNTs on thermal properties

The impacts of the CNTs on the thermal stability of the synthetised membranes were studied by TGA and DSC. Samples with 1 wt% CNT mass fraction are shown in Fig. 6 to compare the weight loss processes. The first step involved a weight loss for all samples occurring below 130°C, which was attributed to the evaporation of the absorbed water in the MMMs. The next two weight loss stages in the temperature ranges of 250-370 °C and 370-550 °C were attributed to the elimination of side groups of PVA and the degradation of the PVA backbone [45]. The main decomposition of PVA commenced at 271 °C, and that temperature increased to 277 °C and 280 °C for PVA/MWCNT and PVA/C-MWCNT, respectively. Thermal stability was further improved with the emergence of covalent linkages between PVA, C-MWCNT and MA. A significant increase in the amount of residual material at 800°C (25 wt% for PVA/MA and 40 wt% for PVA/C-MWCNT/MA) compared with the blending membranes was observed. Accordingly, the glass transition temperatures (T_g) were obtained from the DSC results (Fig.7) with the pure PVA membrane exhibiting a T_g of 70.9 °C, whereas for the PVA/MWCNT and PVA/C-MWCNT composites, the T_g increased to 74.6 °C and 81.6 °C, respectively. The PVA/C-MWCNT/MA composite had the highest T_g of 108.4 °C. Further T_g results for all the PVA/CNT samples are presented in Table 1. It has been previously reported that the incorporation of nanofillers restrains the mobility of the polymer chains and prohibits “free radical transfer”, thus enhancing the thermal stability [46, 47]. Both the TGA and DSC results in this study confirmed that the PVA/CNT composites exhibited higher thermal stability than pure PVA. In addition, compared with PVA/MWCNT samples, PVA/C-MWCNT had a better thermal stability as a result of uniform dispersion and stronger interfacial interaction with PVA.

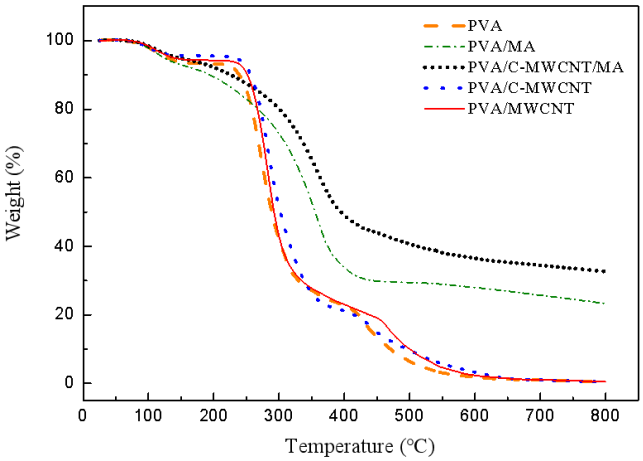

Fig. 6. TGA curves of the pure PVA and the PVA/CNT membranes.

Table 1

Tg, ΔHm, Xc versus CNTs loading for PVA and its composite membranes.

Sample type	CNT loading (wt%)	Tg	ΔHm (Jg^{-1})	χc (%)
Pure PVA	-	70.9 ± 1.5	45.7 ± 0.7	33.0 ± 0.5
PVA/MA	-	94.7 ± 1.2	21.2 ± 0.6	15.3 ± 0.4
PVA/MWCNT	0.5	73.5 ± 1.3	42.8 ± 0.7	30.9 ± 0.5
	1	74.6 ± 1.1	46.1 ± 0.4	33.3 ± 0.3
	2	76.6 ± 1.4	49.6 ± 0.5	35.9 ± 0.4
PVA/C-MWCNT	0.5	79.2 ± 1.1	42.6 ± 0.3	30.7 ± 0.2
	1	81.6 ± 1.3	48.5 ± 0.6	35.1 ± 0.4
	2	84.9 ± 1.5	59.4 ± 0.7	42.9 ± 0.5
PVA/C-MWCNT/MA	0.5	97.4 ± 1.2	11.6 ± 0.4	8.4 ± 0.3
	1	108.4 ± 1.4	13.5 ± 1.04	10.2 ± 0.3
	2	114.2 ± 1.5	16.5 ± 0.8	11.9 ± 0.6

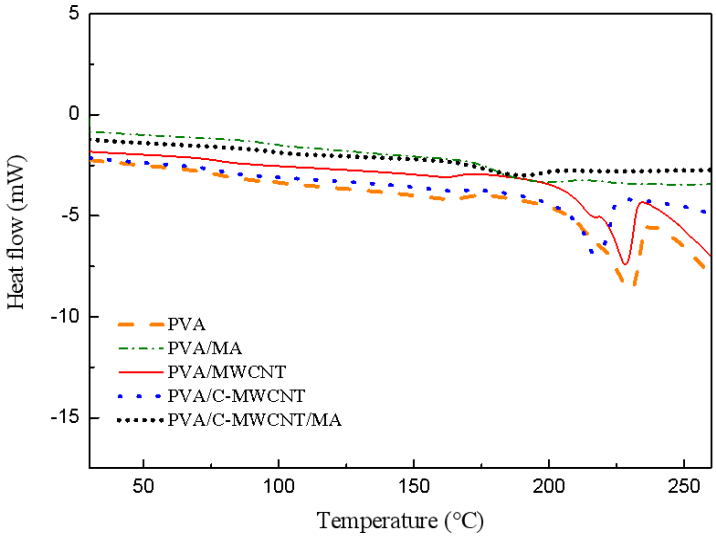

Fig. 7. DSC curves of the pure PVA and the PVA/CNT membranes.

3.3.2. Polymer matrix crystallinity

To further investigate the effect of CNT mass fraction on the degree of crystallinity, the melting enthalpy and degree of crystallinity are listed in Table 1. For the blending membranes, when the mass fraction of CNTs in PVA polymer was 0.5 %, the degree of crystallinity slightly decreased from 33% (PVA) to 30.9 % (PVA/MWCNT) and 30.8 % (PVA/C-MWCNT). Previous literature [48, 49] has reported that carbon nanotubes can promote the crystallinity of polymers by acting as nucleation sites. When the CNTs act as nucleation sites, the interactions between CNTs and PVA may interrupt the original chain packing of PVA and induce PVA molecules to orient into particular conformations around the CNT surfaces that in turn influences adjacent PVA chains [49]. When the content of CNTs was low in polymer matrix, the degree of crystallinity was lower than pure PVA because there were

insufficient nucleation sites. However, it can be seen in Table 1 that the degrees of crystallinity were enhanced by increasing the CNTs mass fraction. Compared with PVA/MWCNT membrane, PVA/C-MWCNT membrane had a higher degree of crystallinity with 1 wt% and 2 wt% CNTs loadings. This was mainly because the dispersion of C-MWCNTs was much better than MWCNTs with a greater available interface area for chain packing around the CNTs (> 2.5-10 m^2/g of membrane assuming the CNTs dispersed individually). For the crosslinked membranes (PVA/MA and PVA/C-MWCNT/MA), esterification reaction may disrupt the chain packing or react with the PVA chains before they can crystallise, resulting in increased amorphous regions, and thus the degree of crystallinity was significantly decreased. It can still be seen that even though PVA polymer chains were covalently connected, the crystallinity of PVA/C-MWCNT/MA was enhanced by increasing C-MWCNTs content.

Further investigation of crystallite size was explored using WAXD characterisation of 1 wt% CNTs to PVA as shown in Fig. 8. Pure PVA and composite membranes all exhibited a strong peak intensity for XRD at $2\theta = 19.5^{\circ}$. The full width at half maximum (FWHM) can be used as an indication of crystallite size, with broader peak widths being indicative of a smaller crystallite size. As shown in Table 2, the crystallite size of PVA/MWCNT membrane was the largest (4.1 ± 0.31 nm), whereas that of PVA/C-MWCNT (3.1 ± 0.07 nm) was smaller. The reason was that the heat treatment at 140 □ was higher than the T_g for all the PVA/CNT composites allowing the PVA molecules to rearrange and form a crystalline phase. The existence of -COOH on C-MWCNTs may disorder the PVA chain packing compared with CNTs without functional groups, and also result in lower the crystal growth velocity [50]. Crystallization was further diminished by crosslinking and consequently, the average crystallite size was the smallest among all the PVA/CNT composites.

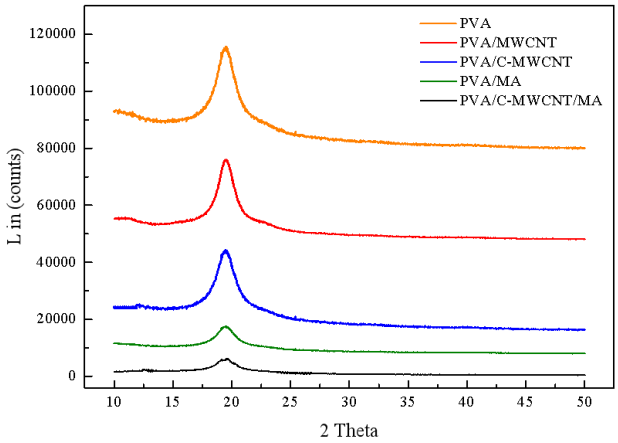

Fig. 8. XRD patterns of the pure PVA and the PVA/CNT membranes.

Table 2

Crystallite sizes of PVA and its composite membranes.

Sample type	FWHM （° 2θ）	Crystallite Size (nm)
Pure PVA	1.6 ± 0.1	3.2 ± 0.03
PVA/MA	2.1 ± 0.1	2.3 ± 0.05
PVA/MWCNT	1.4 ± 0.1	4.1 ± 0.31
PVA/C-MWCNT	1.8 ± 0.1	3.1 ± 0.07
PVA/C-MWCNT/MA	2.3 ± 0.1	2.1 ± 0.08

3.4. Surface hydrophilic properties of synthesized membranes

Fig. 9 shows the water contact angles for the different membranes. For the blending membranes, the water contact angles were increased by 30 % (PVA/MWCNT, 0.5 wt% of MWCNT) and 20 % (PVA/C-MWCNT, 0.5 wt% of C-MWCNT) compared with pure PVA. The water contact angles increased as the content of CNTs was increased from 0.5 wt% to 2 wt%. As MWCNTs are hydrophobic,

the incorporation of MWCNTs into hydrophilic PVA matrix would inevitably reduce the contact between PVA and water molecules, thus increasing water contact angle values [51] [52]. For the PVA/C-MWCNT membrane, the -COOH groups on MWCNTs are hydrophilic although not as hydrophilic as PVA (water contact angle for C-MWCNT was 70.8 ± 2°). Another reason was that the growing crystallinity of PVA with the addition of CNTs affected the surface hydrophilicity [14]. The PVA crystallites were impermeable, which will diminish the amount of water molecules adsorbed into the membrane [52]. As for PVA/MA and PVA/C-MWCNT/MA membranes, the significant increase of water contact angle was due to the consumption of hydrophilic groups by esterification reaction and the surface hydrophilicity was further weakened by increasing the C-MWCNT mass fraction resulting from higher crosslinking density.

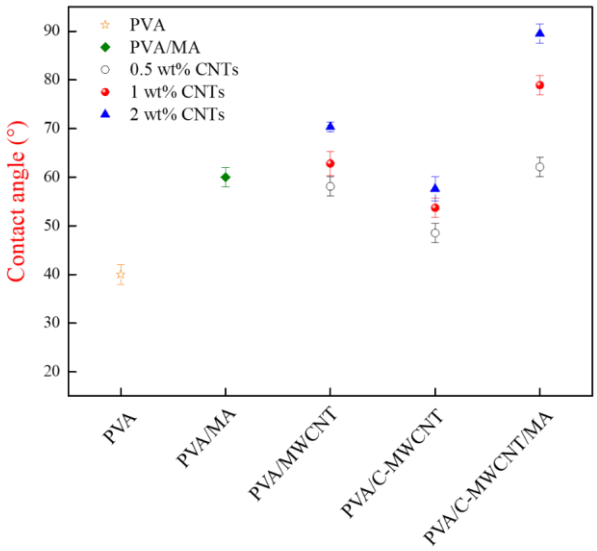

Fig. 9. Contact angle results of the pure PVA and the PVA/CNT membranes with different CNTs loading.

3.5. Swelling study

In Fig. 10, the amount of swelling of pure PVA when immersed in water was 300 ± 5% and that of PVA/MA was 63 ± 5%. This suggested that the swelling behaviour of PVA was significantly restrained by covalent linkages formed between MA and PVA. It is understandable that the swelling would be further decreased by increasing crosslinking density with both MA and C-MWCNTs for the PVA/C-MWCNT/MA membrane. There was no difference between the swelling of pure PVA and PVA/MWCNT membrane when 0.5 wt% of MWCNT was added. However, the swelling of PVA/MWCNT membrane decreased from 267±5% to 249±5% with an increase in the content of MWCNT as a result of enhanced crystallinity of the PVA matrix. For the PVA/C-MWCNT membrane, the trend was similar to PVA/MWCNT membrane but with a decreased level of swelling. In addition to the elevation of crystallinity of PVA/C-MWCNT membrane, there was also a stronger interfacial interaction, i.e. hydrogen bonding, between -COOH and -OH, resulting in suppression of polymer chain mobility [53, 54]. That also contributed to restraining membrane swelling in water [27].

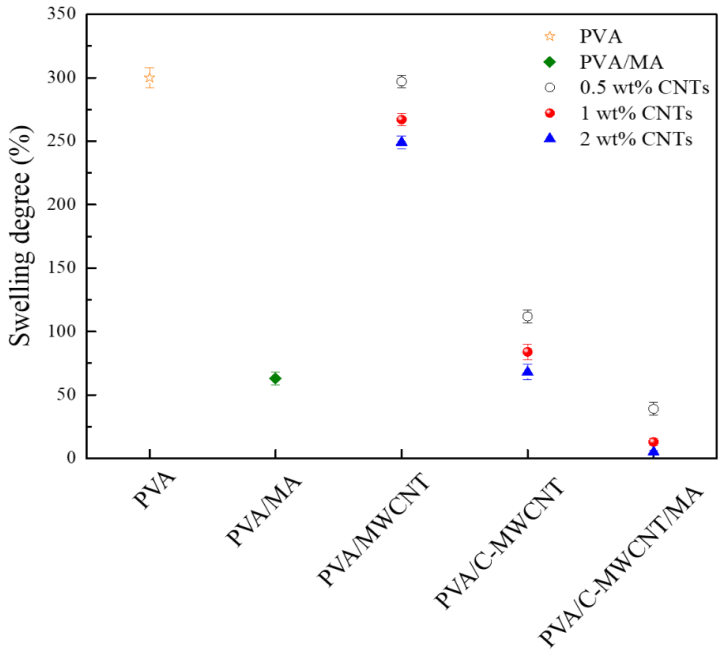

Fig. 10. Swelling of the pure PVA and the PVA/CNT membranes with different CNTs loading.

3.6. Desalination performance

3.6.1. Performance comparison of PVA/CNT membranes

Fig. 11 depicts the PV flux and salt rejection of the synthesized membranes with a feed temperature of 55 °C. The result shows that the PVA/CNT membranes all had higher water fluxes than the PVA/MA membrane (38.8% to 154.1% increase of water flux compared to the PVA/MA membrane). The PVA/C-MWCNT membrane had the highest water flux of 21.66 kg/m^2 h, and PVA/MWCNT and PVA/C-MWCNT/MA membranes exhibited 15.75 kg/m^2 h and 11.86 kg/m^2 h, respectively. For the PVA/CNT membranes, the water transport mechanism imparted by CNTs has

been altered compared with the diffusion in polymer membrane. The presence of CNTs provided large area of aromatic structures composed of hexagonal carbon lattice. This unique construction of morphology is hydrophobic and has been shown to have no impediment for water transport [32, 55-60]. Thus, the incorporation of CNTs into the polymer matrix can lower the overall water transport resistance of the MMMs [61].

For PVA/MWCNT and PVA/C-MWCNT composite membranes, the water flux was significantly affected by the dispersion of CNTs in the polymer. As shown previously in TEM and SEM images in Fig. 2 and Fig. 3, respectively, the majority of MWCNTs formed bundles or entanglements in the PVA matrix. The formation of aggregated CNTs isolated the nanofillers from the polymer matrix, leading to a reduction of the interface area between the nanofiller and PVA. However, the C-MWCNTs were dispersed more uniformly, and therefore there were larger interfacial areas. Another reason for the higher water flux of PVA/C-MWCNT membrane was the existence of -COOH. PVA/C-MWCNT membrane was more hydrophilic than PVA/MWCNT membrane, which allowed it to adsorb more water during the PV process. In addition, the homogeneous distribution of charged groups within the polymer matrix as fixed sites also facilitated water transport [62]. Therefore, all these factors contributed to the fast water transport of PVA/C-MWCNT membrane. For the PVA/C-MWCNT/MA membrane, a significant flux decline was observed which may be due to the steric hinderance from the crosslinked network. Although the -COOH groups were converted to ester groups, the intact frictionless surface of carbon nanotubes remained and connected to the crosslinked network. The water molecules can therefore slide along the unoxidized regions of C-MWCNTs that are otherwise impeded by the non-slip behaviour of the polymer membrane without CNTs [63].

For non-porous polymer membranes, the free volume has a major impact on water flux and salt

rejection [14], whereby the free volume of a swollen membrane would be occupied by water molecules. Salts can be dissolved in the membrane in the shell of water molecules if there is enough space for accommodation. Therefore, the kinetic desorption method was combined with water uptake to explain the salt transport properties of the synthesized membranes and the results for NaCl diffusivities and NaCl solubilities of the various membrane types are shown in Fig.12. For all the PVA/CNT membranes, the NaCl solubility was monotonically increasing with swelling, indicating that the NaCl solubility was affected by the water content in the membranes. For the NaCl diffusivity, it can be observed that all the membranes at 2 wt% of CNTs loading had the highest diffusivities. According to the SEM and TEM results, the reason could be attributed to the agglomeration of CNTs. The cluster of CNTs in polymer matrix may result in unexpected defects such as non-selective interfacial voids. As a consequence, the occurrence of such voids could disable the selectivity of membrane. Particularly, the NaCl diffusivity of PVA/MWCNT membrane was proportionally increasing with MWCNT mass fraction. Considering the dispersion state of MWCNTs in polymer matrix, estimation could be made that increasing the loading of MWCNTs may induce more defects. On the other hand, the dispersion of C-MWCNTs in PVA was homogeneous, and the NaCl diffusivity decreased when CNTs loading increased from 0.5 wt% to 1 wt%.

For the overall NaCl permeability, it increased from 9.6×10^{-6} to 13.9×10^{-6} cm^2/s with CNT loading for the PVA/MWCNT membrane, indicating the incorporation of MWCNTs had negative effect on salt rejection. For example, when the mass fraction of CNTs was 0.5 wt%, the calculated NaCl permeability of PVA/MWCNT membrane was higher than those of PVA/MA (7.7×10^{-6} cm^2/s), PVA/C-MWCNT (6.8×10^{-6} cm^2/s) and PVA/C-MWCNT/MA (1.7×10^{-6} cm^2/s). Accordingly, the salt rejection of PVA/MWCNT was the lowest and the PVA/C-MWCNT/MA membrane had the

highest salt rejection. For the PVA/C-MWCNT and PVA/C-MWCNT/MA membranes, the NaCl permeability decreased from 6.8×10^{-6} to 2.8×10^{-6} cm^2/s and 1.7×10^{-6} to 0.5×10^{-6} cm^2/s with CNT loading (0.5 wt% to 1 wt%), respectively. However, the NaCl permeability increased to 5.1×10^{-6} cm^2/s for the PVA/C-MWCNT membrane and 2.2×10^{-6} cm^2/s for the PVA/C-MWCNT/MA membrane when CNTs loading was 2 wt%. That could be owing to the formation of aggregation of CNTs as discussed above.

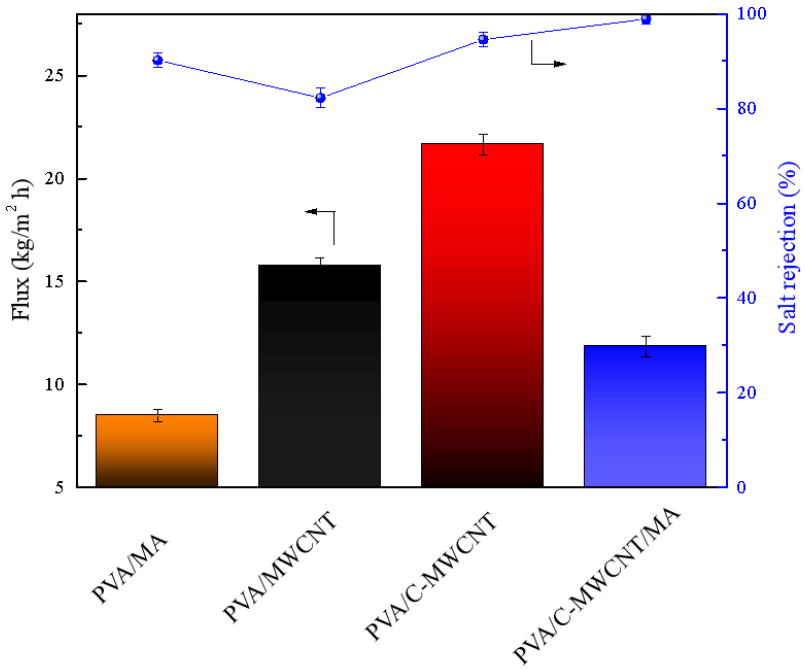

Fig. 11. PVA/CNT membrane desalination performance (0.5 wt% of CNTs loading).

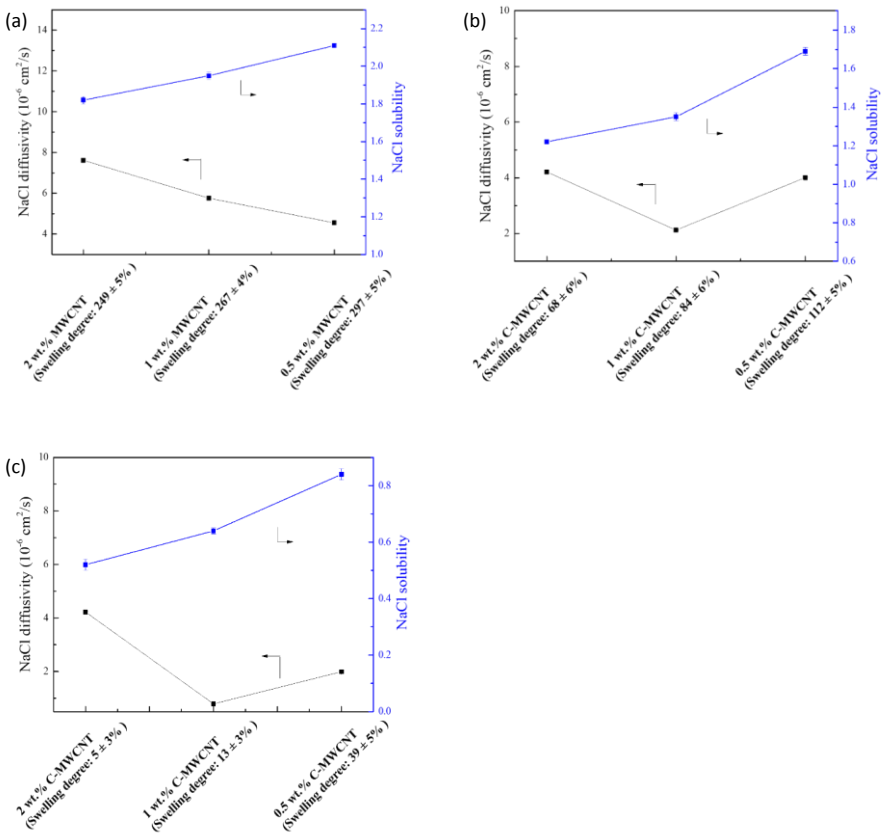

Fig. 12. Relationship between swelling and NaCl diffusivity and solubility of (a) PVA/MWCNT, (b) PVA/C-MWCNT and (c) PVA/C-MWCNT/MA.

3.6.2. Effect of CNT loading on desalination performance

To avoid consideration of defects, the following analysis is focused on the comparison between PVA/C-MWCNT and PVA/C-MWCNT/MA membranes. Fig. 13 shows the desalination performance of PVA/C-MWCNT membrane versus CNT content at room temperature. It can be seen that both the flux and salt rejection were enhanced when the mass fraction of C-MWCNT was increased from 0.5

wt% to 1 wt%. However, the salt rejection decreased significantly to 89.21% at the CNT loading of 2 wt% and the water flux increased significantly. This was in accordance with kinetic desorption results discussed above. For PVA/C-MWCNT/MA membrane in Fig. 14, the decline of flux at 1 wt% CNT loading can be attributed to the increased interconnections or the grafting of PVA chains that resulted from the elevation of CNT mass fraction compared with PVA/C-MWCNT/MA membrane with 0.5 wt% C-MWCNT loading and the best salt rejection (99.91%) was achieved. Similar to the result of the PVA/CNT blended membranes, when 2 wt% C-MWCNT was incorporated, salt rejection decreased to 95.2% and the flux increased to 8.64 kg/m^{2}h due to the formation of agglomerated CNTs.

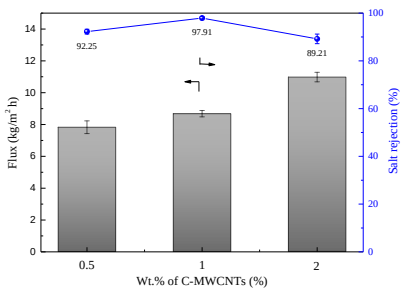

Fig. 13. PVA/C-MWCNT membrane performance.

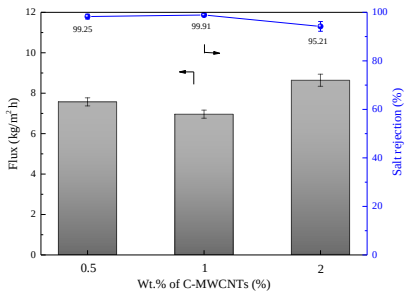

Fig. 14. PVA/C-MWCNT/MA membrane performance.

3.6.3. Membrane durability tests

Unprocessed seawater was collected from Brighton Beach (Melbourne, VIC, Australia) for the long-term stability tests. The temperature of seawater was maintained at room temperature for 30 h duration of the test. Fig. 15 (a) shows the results of the long-term flux and salt rejection for the PVA/C-MWCNT membrane (1 wt% C-MWCNTs loading). It is worth noting that the restrained swelling and enhanced crystallinity degree prohibited the ~~dissolving~~ dissolution of PVA during the pervaporation

test, t~~. T~~hus, the performance is valid for the blended PVA/C-MWCNT membrane. In the first 8 h, the flux decreased continuously, possibly because some fouling contaminants such as natural organic matter deposited on the surface of the membrane. After 8 h, the flux started to increase while the salt rejection dropped dramatically. In this case, the structure of the PVA/C-MWCNT membrane may have been damaged by continuous water processing and fouling. Whereas over the whole operating duration, as shown in Fig.15 (b), the PVA/C-MWCNT/MA (1 wt% C-MWCNTs loading) exhibited a more stable performance with only 7.58 % flux decrease and the salt rejection remained in the range of 99.8% to 99.6%. It should be noted that the inner diameter of the CNTs used in this research were 2-5 nm, which was far larger than the diameters of water molecular (≈0.29 nm) [64] and hydrated ions such as 0.66 nm for K^+, 0.66 nm for Cl^-, 0.72 nm for Na^+, 0.76 nm for SO_4^{2-}, 0.82 nm for Ca^{2+}, and 0.86 nm for Mg^{2+} [65]. The reason why the high salt rejection of PVA/C-MWCNT/MA was retained may be the restrained swelling of the PVA, good dispersion of C-MWCNTs and the subsequent interactions with the polymer. Disentanglement of CNTs may lead to the blocking of the open ends by the polymer and thus reducing the effective diameter of CNTs. Similar results were also reported by Kim et al [34]. Another explanation is that after covalently grafting or attaching a long functional group on the CNTs, the groups tended to fold into the tube due to the flexibility and lower energy state [36]. Finally, a simplified schematic illustration demonstrating water permeation through the PVA/C-MWCNT/MA membrane using NaCl solution as feed is proposed in Fig.16. Covalent bonding between PVA and C-MWCNT or MA, or the grafting of the PVA chains onto the C-MWCNTs results in an interconnected network, which effectively controls the swelling. According to the solution-diffusion model, water molecules are firstly adsorbed onto the membrane surface and then diffused through the membrane. The immobilized C-MWCNTs in the matrix provide an altered transport mechanism due to its unique

Commented [MC1]: I would start this as a new paragraph and place after figure 15.

morphology structure and physicochemical properties. At first, water molecules could be inserted into the hollow space of C-MWCNTs by capillary force [66] and pass through with low friction, which is marked as path 1 in Fig. 16. For path 2, as C-MWCNTs have high aspect ratio and hydrophilic groups, water molecules also tend to be rapidly adsorbed and desorbed [35] [67, 68], resulting in a fast diffusion along the outside surface. Furthermore, it should be noted that the space between each rolled graphene in MWCNT is 0.34 nm [69]. That structure may potentially provide multilayered transport channels similar to those of reduced graphene oxide. For the region without C-MWCNTs, the permeation is through the free volume of the crosslinked PVA as shown in path 3. Finally, a tiny amount of salts may also permeate through the membrane as illustrated in the salt transport properties. It should also be noted that considering the real distribution of the C-MWCNTs, the transport of water molecules should be more complicated than the schematics shown here.

Commented [MC2]: graphene tube?

Commented [MC3]: minimal?

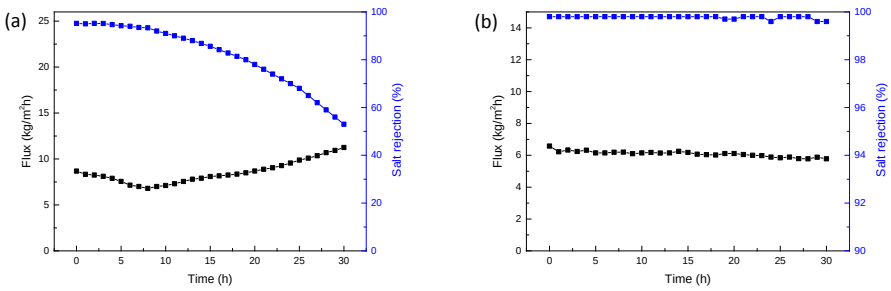

Fig. 15. Long term tests of (a) PVA/C-MWCNT membrane and (b) PVA/C-MWCNT/MA membrane using seawater (1 wt% of C-MWCNTs loading).

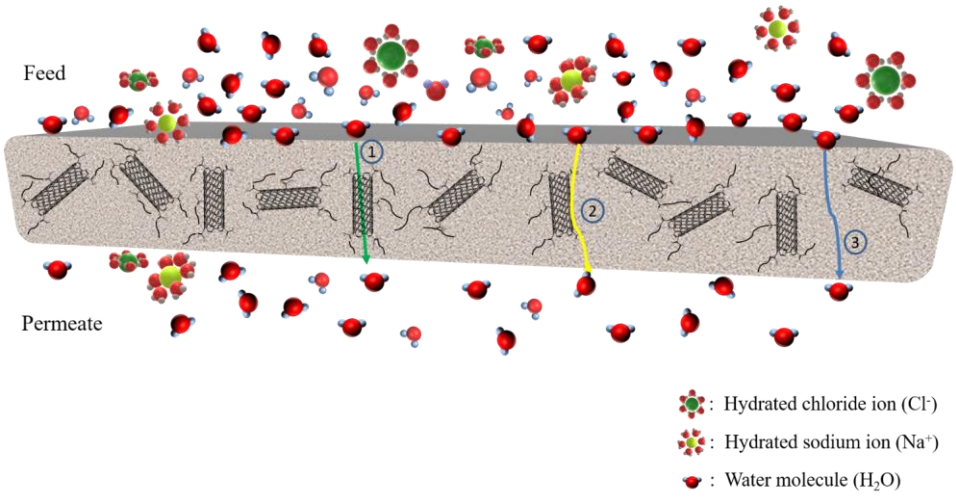

Fig.16. Proposed schematic illustration of water permeation through PVA/C-MWCNT/MA membrane. ①: water transport through CNT central pore; ②: water transport along outside surface of CNT; ③: water transport through PVA.

4. Conclusions

In this study, for the first time, three types of MMMs comprised of PVA and different MWCNTs; i.e. PVA/MWCNT, PVA/C-MWCNT and PVA/C-MWCNT/MA for desalination using the PV process were fabricated and compared. Different interactions between the CNTs and the PVA, i.e. interfacial adhesion, hydrogen bonding and covalent linkage resulted in enhancements in the physicochemical and structural properties, especially for the separation characteristics. The carboxylic groups improved the dispersion of C-MWCNTs and resulted in a uniform distribution in the polymer matrix whereas the MWCNTs were prone to agglomeration. The improvement of the PVA/CNT membranes was observed by increases in water flux between 38.8% to 154.1% compared with the control PVA/MA membrane while maintaining a relatively high salt rejection. Kinetic desorption of NaCl revealed that

the salt transport behaviour was significantly affected by the dispersion of CNTs and swelling. When CNTs aggregated, the selectivity of the PVA/CNT membrane diminished. By forming an interconnected network, the PVA/C-MWCNT/MA composite membrane was able to obtain a total salt rejection of over 99.8 % at room temperature using synthetic NaCl solution as feed and good long-term stability for processing seawater for 30 h. Overall, this work improves the understanding of the structure-property relationships of MMMs and the rational design of separation orientated functional membranes.

Acknowledgments

The authors would like to acknowledge the financial support from Victoria University and CSIRO Manufacturing. Guang Yang gratefully acknowledges the scholarship from China Scholarship Council (CSC). Special thanks are given to Dr. Mark Greaves (CSIRO) and Dr. Malisja de Vries (CSIRO) for the SEM training, Dr. Jacinta White (CSIRO) for TEM tests, Dr. Yesim Gozukara (CSIRO) for TGA and DSC training, and Dr. Aaron Seeber (CSIRO) for XRD tests in this work.

References

[1] L.F. Greenlee, D.F. Lawler, B.D. Freeman, B. Marrot, P. Moulin, Reverse osmosis desalination: water sources, technology, and today's challenges, Water Res, 43 (2009) 2317-2348.

[2] A.W. Mohammad, Y.H. Teow, W.L. Ang, Y.T. Chung, D.L. Oatley-Radcliffe, N. Hilal, Nanofiltration membranes review: Recent advances and future prospects, Desalination, 356 (2015) 226-254.

[3] J.R. Varcoe, P. Atanassov, D.R. Dekel, A.M. Herring, M.A. Hickner, P.A. Kohl, A.R. Kucernak, W.E. Mustain, K. Nijmeijer, K. Scott, T. Xu, L. Zhuang, Anion-exchange membranes in electrochemical energy systems, Energy Environ. Sci., 7 (2014) 3135-3191.

[4] A. Alkhudhiri, N. Darwish, N. Hilal, Membrane distillation: A comprehensive review, Desalination, 287 (2012) 2-18.

[5] L. Gao, J. Zhang, S. Gray, J.-D. Li, Experimental study of hollow fiber permeate gap membrane distillation and its performance comparison with DCMD and SGMD, Separation and Purification Technology, 188 (2017) 11-23.

[6] L. Gao, J. Zhang, S. Gray, J.-D. Li, Influence of PGMD module design on the water productivity and energy efficiency in desalination, Desalination, 452 (2019) 29-39.

[7] Q. Wang, N. Li, B. Bolto, M. Hoang, Z. Xie, Desalination by pervaporation: A review, Desalination, 387 (2016) 46-60.
[8] E. Korin, I. Ladizhensky, E. Korngold, Hydrophilic hollow fiber membranes for water desalination by the pervaporation method, Chemical Engineering and Processing, 35 (1996) 451-457.
[9] Y.K. Ong, G.M. Shi, N.L. Le, Y.P. Tang, J. Zuo, S.P. Nunes, T.-S. Chung, Recent membrane development for pervaporation processes, Progress in Polymer Science, 57 (2016) 1-31.
[10] J.G. Wijmans, R.W. Baker, The solution-diffusion model: a review, Journal of Membrane Science 107 (1995) 1-21.
[11] C. Fritzmann, J. Löwenberg, T. Wintgens, T. Melin, State-of-the-art of reverse osmosis desalination, Desalination, 216 (2007) 1-76.
[12] B. Liang, W. Zhan, G. Qi, S. Lin, Q. Nan, Y. Liu, B. Cao, K. Pan, High performance graphene oxide/polyacrylonitrile composite pervaporation membranes for desalination applications, Journal of Materials Chemistry A, 3 (2015) 5140-5147.
[13] Q. Wang, Y. Lu, N. Li, Preparation, characterization and performance of sulfonated poly(styrene-ethylene/butylene-styrene) block copolymer membranes for water desalination by pervaporation, Desalination, 390 (2016) 33-46.
[14] Z. Xie, M. Hoang, T. Duong, D. Ng, B. Dao, S. Gray, Sol–gel derived poly(vinyl alcohol)/maleic acid/silica hybrid membrane for desalination by pervaporation, Journal of Membrane Science, 383 (2011) 96-103.
[15] Y. Li, G. He, S. Wang, S. Yu, F. Pan, H. Wu, Z. Jiang, Recent advances in the fabrication of advanced composite membranes, Journal of Materials Chemistry A, 1 (2013) 10058.
[16] A.F. Ismail, P.S. Goh, S.M. Sanip, M. Aziz, Transport and separation properties of carbon nanotube-mixed matrix membrane, Separation and Purification Technology, 70 (2009) 12-26.
[17] Z. Wang, D. Wang, S. Zhang, L. Hu, J. Jin, Interfacial Design of Mixed Matrix Membranes for Improved Gas Separation Performance, Adv Mater, 28 (2016) 3399-3405.
[18] S. Khoonsap, S. Rugmai, W.-S. Hung, K.-R. Lee, S. Klinsrisuk, S. Amnuaypanich, Promoting permeability-selectivity anti-trade-off behavior in polyvinyl alcohol (PVA) nanocomposite membranes, Journal of Membrane Science, 544 (2017) 287-296.
[19] I. Jesswein, T. Hirth, T. Schiestel, Continuous dip coating of PVDF hollow fiber membranes with PVA for humidification, Journal of Membrane Science, 541 (2017) 281-290.
[20] Z. Xie, D. Ng, M. Hoang, T. Duong, S. Gray, Separation of aqueous salt solution by pervaporation through hybrid organic–inorganic membrane: Effect of operating conditions, Desalination, 273 (2011) 220-225.
[21] C.H. Cho, K.Y. Oh, S.K. Kim, J.G. Yeo, P. Sharma, Pervaporative seawater desalination using NaA zeolite membrane: Mechanisms of high water flux and high salt rejection, Journal of Membrane Science, 371 (2011) 226-238.
[22] S.M. Hosseini, M. Nemati, F. Jeddi, E. Salehi, A.R. Khodabakhshi, S.S. Madaeni, Fabrication of mixed matrix heterogeneous cation exchange membrane modified by titanium dioxide nanoparticles: Mono/bivalent ionic transport property in desalination, Desalination, 359 (2015) 167-175.
[23] D.Q. Vu, W.J. Koros, S.J. Miller, Mixed matrix membranes using carbon molecular sieves I. Preparation and experimental results, Journal of Membrane Science, 211 (2003) 311-334.
[24] J.R. Li, J. Sculley, H.C. Zhou, Metal-organic frameworks for separations, Chem Rev, 112 (2012) 869-932.
[25] J. Yin, B. Deng, Polymer-matrix nanocomposite membranes for water treatment, Journal of Membrane Science, 479 (2015) 256-275.
[26] H. Xu, M. Ding, S. Liu, Y. Li, Z. Shen, K. Wang, Preparation and characterization of novel polysulphone hybrid ultrafiltration membranes blended with N-doped GO/TiO 2 nanocomposites, Polymer, 117 (2017) 198-207.
[27] Y. Shirazi, M.A. Tofighy, T. Mohammadi, Synthesis and characterization of carbon nanotubes/poly vinyl alcohol nanocomposite membranes for dehydration of isopropanol, Journal of Membrane Science, 378 (2011) 551-561.
[28] P.-C. Ma, N.A. Siddiqui, G. Marom, J.-K. Kim, Dispersion and functionalization of carbon nanotubes for polymer-based nanocomposites: A review, Composites Part A: Applied Science and Manufacturing, 41 (2010) 1345-1367.
[29] R.H. Baughman, A.A. Zakhidov, W.A.d. Heer, Carbon Nanotubes—the Route Toward Applications, Science, 297

(2002) 787-792.
[30] M. Majumder, N. Chopra, R. Andrews, B.J. Hinds, Enhanced flow in carbon nanotubes, Nature, 438 (2005) 44.
[31] J.K. Holt, H.G. Park, Y. Wang, M. Stadermann, A.B. Artyukhin, C.P. Grigoropoulos, A. Noy, O. Bakajin, Fast Mass Transport Through Sub–2-Nanometer Carbon Nanotubes, Science, 312 (2006) 1034-1037.
[32] G. Hummer, J.C. Rasaiah, J.P. Noworyta, Water conduction through the hydrophobic channel of a carbon nanotube, Nature, 414 (2001) 188-190.
[33] S. Li, G. Liao, Z. Liu, Y. Pan, Q. Wu, Y. Weng, X. Zhang, Z. Yang, O.K.C. Tsui, Enhanced water flux in vertically aligned carbon nanotube arrays and polyethersulfone composite membranes, J. Mater. Chem. A, 2 (2014) 12171-12176.
[34] H.J. Kim, K. Choi, Y. Baek, D.G. Kim, J. Shim, J. Yoon, J.C. Lee, High-performance reverse osmosis CNT/polyamide nanocomposite membrane by controlled interfacial interactions, ACS Appl Mater Interfaces, 6 (2014) 2819-2829.
[35] K. Gethard, O. Sae-Khow, S. Mitra, Water desalination using carbon-nanotube-enhanced membrane distillation, ACS Appl Mater Interfaces, 3 (2011) 110-114.
[36] W.F. Chan, H.Y. Chen, A. Surapathi, M.G. Taylor, X. Shao, E. Marand, J.K. Johnson, Zwitterion Functionalized Carbon Nanotube/Polyamide Nanocomposite Membranes for Water Desalination, ACS NANO, 7 (2013) 5308-5319.
[37] B. Corry, Water and ion transport through functionalised carbon nanotubes: implications for desalination technology, Energy & Environmental Science, 4 (2011) 751.
[38] H.-C. Yang, J. Hou, V. Chen, Z.-K. Xu, Surface and interface engineering for organic–inorganic composite membranes, Journal of Materials Chemistry A, 4 (2016) 9716-9729.
[39] J.M. Gohil, A. Bhattacharya, P. Ray, Studies on the Cross-linking of Poly(Vinyl Alcohol), Journal of Polymer Research, 13 (2006) 161–169.
[40] B. Wang, Z. Chen, J. Zhang, J. Cao, S. Wang, Q. Tian, M. Gao, Q. Xu, Fabrication of PVA/graphene oxide/TiO2 composite nanofibers through electrospinning and interface sol–gel reaction: Effect of graphene oxide on PVA nanofibers and growth of TiO2, Colloids and Surfaces A: Physicochemical and Engineering Aspects, 457 (2014) 318-325.
[41] H. Ju, A.C. Sagle, B.D. Freeman, J.I. Mardel, A.J. Hill, Characterization of sodium chloride and water transport in crosslinked poly(ethylene oxide) hydrogels, Journal of Membrane Science, 358 (2010) 131-141.
[42] Z. Xie, M. Hoang, D. Ng, C. Doherty, A. Hill, S. Gray, Effect of heat treatment on pervaporation separation of aqueous salt solution using hybrid PVA/MA/TEOS membrane, Separation and Purification Technology, 127 (2014) 10-17.
[43] E.M. Pérez, N. Martín, π–π interactions in carbon nanostructures, Chemical Society Reviews, 44 (2015) 6425-6433
[44] L. Zhang, J. Wang, C.A. Fuentes, D. Zhang, A.W. Van Vuure, J.W. Seo, D. Seveno, Wettability of carbon nanotube fibers, Carbon, 122 (2017) 128-140.
[45] A. Ballistreri, S. Foti, G. Montaudo, E. Scamporrino, Evolution of Aromatic Compounds in the Thermal Decomposition of Vinyl Polymers, Journal of Polymer science: Polymer Chemistry, 18 (1980) 1147-1153.
[46] Z.H. Mbhele, M.G. Salemane, C.G.C.E.v. Sittert, J.M. Nedeljkovic, V. Djokovic, a.A.S. Luyt, Fabrication and Characterization of Silver-Polyvinyl Alcohol Nanocomposites, Chem. Mater., 15 (2003) 5019-5024.
[47] D. Sajinovic, Z.V. Saponji, N. Cvjeticanin, M. Marinovic, Cincovic, J.M. Nedeljkovic, Synthesis and characterization of CdS quantum dots±polystyrene composite, Chemical Physics Letters, 329 (2000) 168-112.
[48] W. Chen, X. Tao, P. Xue, X. Cheng, Enhanced mechanical properties and morphological characterizations of poly(vinyl alcohol)–carbon nanotube composite films, Applied Surface Science, 252 (2005) 1404-1409.
[49] J.N. Coleman, M. Cadek, R. Blake, V. Nicolosi, K.P. Ryan, C. Belton, A. Fonseca, J.B. Nagy, Y.K. Gun'ko, W.J. Blau, High Performance Nanotube-Reinforced Plastics: Understanding the Mechanism of Strength Increase, Advanced Functional Materials, 14 (2004) 791-798.
[50] F. Pilati, M. Toselli, M. Messori, C. Manzoni, A. Turturro, E.G. Gattiglia, On specific factors affecting the crystallization of PET: the role of carboxyl terminal groups and residual catalysts on the crystallization rate, Polymer, 38 (1997) 4469-4476.

[51] M. Sianipar, S.H. Kim, Khoiruddin, F. Iskandar, G. Wenten, Functionalized carbon nanotube (CNT) membrane: progress and challenges, RSC Adv., 7 (2017) 51175–51198

[52] M. Naebe, T. Lin, W. Tian, L. Dai, X. Wang, Effects of MWNT nanofillers on structures and properties of PVA electrospun nanofibres, Nanotechnology, 18 (2007) 225605.

[53] B. Tan, N.L. Thomas, A review of the water barrier properties of polymer/clay and polymer/graphene nanocomposites, Journal of Membrane Science, 514 (2016) 595-612.

[54] C. Kong, M. Kanezashi, T. Yamomoto, T. Shintani, T. Tsuru, Controlled synthesis of high performance polyamide membrane with thin dense layer for water desalination, Journal of Membrane Science, 362 (2010) 76-80.

[55] X. Liu, X. Pan, S. Zhang, X. Han, X. Bao, Diffusion of water inside carbon nanotubes studied by pulsed field gradient NMR spectroscopy, Langmuir, 30 (2014) 8036-8045.

[56] A. Striolo, The Mechanism of Water Diffusion in Narrow Carbon Nanotubes, Nano Lett, 6 (2006) 633-639.

[57] B.J. Hinds, N. Chopra, T. Rantell, R. Andrews, V. Gavalas, L.G. Bachas, Aligned Multiwalled Carbon Nanotube Membranes, Science, 303 (2004) 62-65.

[58] M. Majumder, N. Chopra, RodneyAndrews, B.J. Hinds, Enhanced flow in carbon nanotubes, Nature, 438 (2005) 44.

[59] J.K. Holt, H.G. Park, Y. Wang, M. Stadermann, A.B. Artyukhin, C.P. Grigoropoulos, A. Noy, O. Bakajin, Fast Mass Transport Through Sub–2-Nanometer Carbon Nanotubes, SCIENCE, 312 (2006) 1037-1037.

[60] S. Joseph, N.R. Aluru, Why Are Carbon Nanotubes Fast Transporters of Water?, Nano Lett, (2008) 452-458.

[61] J.G. Wijmans, R.W. Baker, The solution-diffusion model: a review, Journal of Membrane Science, 107 (1995) 1-21.

[62] B. Liang, Q. Li, B. Cao, P. Li, Water permeance, permeability and desalination properties of the sulfonic acid functionalized composite pervaporation membranes, Desalination, 433 (2018) 132-140.

[63] D. Mattia, H. Leese, K.P. Lee, Carbon nanotube membranes: From flow enhancement to permeability, Journal of Membrane Science, 475 (2015) 266-272.

[64] J. Yang, D. Gong, G. Li, G. Zeng, Q. Wang, Y. Zhang, G. Liu, P. Wu, E. Vovk, Z. Peng, X. Zhou, Y. Yang, Z. Liu, Y. Sun, Self-Assembly of Thiourea-Crosslinked Graphene Oxide Framework Membranes toward Separation of Small Molecules, Adv Mater, 30 (2018) e1705775.

[65] R.K. Joshi, P. Carbone, F.C. Wang, V.G. Kravets, Y. Su, I.V. Grigorieva, H.A. Wu, A.K. Geim, R.R. Nair, Precise and Ultrafast Molecular Sieving Through Graphene Oxide Membranes, Science, 343 (2014) 752-754.

[66] M. Whitby, N. Quirke, Fluid flow in carbon nanotubes and nanopipes, Nat Nanotechnol, 2 (2007) 87-94.

[67] Z. Dehouche, L. Lafi, N. Grimard, J. Goyette, R. Chahine, The catalytic effect of single-wall carbon nanotubes on the hydrogen sorption properties of sodium alanates, Nanotechnology, 16 (2005) 402–409.

[68] C.M. Hussain, C. Saridara, S. Mitra, Modifying the sorption properties of multi-walled carbon nanotubes via covalent functionalization, Analyst, 134 (2009) 1928-1933.

[69] Y. Saito, T. Yoshikawa, S. Bandow, M. Tomita, T. Hayashi, Interlayer spacings in carbon nanotubes, PHYSICAL REVIEW B, 48 (1993) 1907-1909.